Exploring Homogeneity and Covariance Matrix Structure of Multistatic/Polarimetric Sea-Clutter Data

Carotenuto, V.; Aubry, A.; De Maio, A.; Fioranelli, F.

DOI
10.1109/MetroAeroSpace57412.2023.10190048

Publication date
2023

Document Version
Final published version

Published in
Proceedings of the 2023 IEEE 10th International Workshop on Metrology for AeroSpace (MetroAeroSpace)

Exploring Homogeneity and Covariance Matrix Structure of Multistatic/Polarimetric Sea-Clutter Data

V. Carotenuto, A. Aubry, A. De Maio
DIETI, University of Naples "Federico II"
via Claudio 21, Naples, Italy
{vincenzo.carotenuto, augusto.aubry, ademaio}@unina.it

F. Fioranelli
MS3 Group, Department of Microelectronics, TU Delft
Mekelweg 4, 2628CD Delft, The Netherlands
f.fioranelli@tudelft.nl

2023 IEEE 10th International Workshop on Metrology for AeroSpace (MetroAeroSpace) | 978-1-6654-5690-6/23/$31.00 ©2023 IEEE | DOI: 10.1109/METROAEROSPACE57412.2023.10190048

***Abstract*—The design of bespoke adaptive detection schemes relying on the joint use of multistatic/polarimetric measurements requires a preliminary statistical inference on the clutter interference environment. This is fundamental to develop an analytic model for the received signal samples, which is used to synthesize the radar detector. In this respect, the aim of this paper is the design of suitable learning tools to study some important statistical properties of the sea-clutter environment perceived at the nodes of a multistatic/polarimetric radar system. The study is complemented by the use of radar returns measured with the Netted RADar (NetRAD), which collects simultaneously monostatic and bistatic measurements. Precisely, the homogeneity properties of the data in the slow-time domain are first assessed resorting to Generalized Inner Product (GIP) based statistics. Then, the possible presence of structures in the clutter covariance matrices (both inter and intra channels) is investigated through ad-hoc statistical tools. The results show that the data, regardless the polarimetric/geometric configuration, can be modeled as drawn from a stationary process within the coherence time. Moreover, for both the monostatic and the bistatic returns the structure of the covariance matrix depends upon the polarimetric/geometric configuration of the sensing system.**

***Index Terms*—Multistatic/polarimetric radar, Spherically Invariant Random Process (SIRP), sea-clutter, Generalized Inner Product (GIP), data homogeneity, covariance matrix structure.**

I. Introduction

The design of adaptive detection schemes requires a preliminary statistical inference on the clutter interference environment. This is essential for developing a well-suited analytic model for the received signal, which is used to synthesize the radar detector. Incorrect modeling of the clutter environment can lead to false and/or missed detections, compromising the overall accuracy and effectiveness of the radar system [1], [2].

For multistatic/polarimetric systems the design of adaptive detectors becomes more challenging as it requires the joint characterization of the radar environment perceived at each sensor. Indeed, due to the so called clutter diversity the statistical properties of the interference can differ among the different nodes of the system [3], [4]. Additionally, the analytical model used to synthesize the detector has also to account for the joint use of all the signals collected from the environment. As to the clutter modeling, in [5] a statistical analysis of multistatic/polarimetric sea-clutter returns collected via the Netted RADar (NetRAD) system [6] has been performed. The results highlighted that, over an appropriate time interval (referred to as the coherence time), the considered measurements can be modelled according to a Spherically Invariant Random Process (SIRP) [7]. This is tantamount to describing the clutter backscattering over the coherence time as the product of a nonnegative random variable and a zero-mean circularly symmetric Gaussian process with unknown covariance matrix referred to as texture and speckle, respectively. However, the analyses performed in [5] required the use of uncorrelated slow-time samples and thus no inference on the possible stationarity of the speckle component has been made. For this reason, this paper complements the study conducted in [5] accounting for possible correlations of the slow-time samples composing the observation vector. Precisely, the homogeneity properties of the data in the slow-time domain are first assessed resorting to Generalized Inner Product (GIP) based statistics. Then, the possible presence of structures in the clutter covariance matrices (both inter and intra channels) is investigated through ad-hoc statistical tools. The results show that the data, regardless the polarimetric/geometric configuration, can be modeled as drawn from a stationary process, i.e., they are homogeneous within the coherence time. Moreover, the structure of the covariance matrix associated with the speckle depends upon the polarimetric/geometric configuration of the sensing system.

The remainder of this paper is organized as follows. Section II is devoted to a short description of both the NetRAD system and the radar measurements used in this study. In Section III and IV, for both the monostatic and the bistatic measurements the statistical tools used to assess the data homogeneity and to identify possible structures of the covariance matrix are discussed along with the results obtained using the available measurements, respectively. Finally, in Section V conclusions are drawn and possible future research avenues are pointed out.

II. NetRAD System and Dataset Description

The NetRAD is a S-band ground-based multistatic/polarimetric system allowing the simultaneous collection

978-1-6654-5690-6/23/$31.00 ©2023 IEEE

of both monostatic and bistatic radar returns. It was initially developed by the University College London (UCL) and successively modified via a joint collaboration between UCL and the University of Cape Town (UCT), obtaining separate active and passive nodes with baselines in the order of kilometer. This was achieved synchronizing the entire system using GPS disciplined oscillators (GPSDOs) at each node, thus avoiding cabled connections (as in the original version of the NetRAD) and granting more degrees of freedom in terms of baselines among nodes [6].

Data exploited in this paper were collected on June 9th 2011 in South Africa at Misty Cliffs using three nodes: one active (with transmit and receive capabilities) and two passive (see [8] and [5] for more details). The active node was a pulsed radar operating over a carrier frequency of 2.4 GHz, transmitting linear up-chirp waveforms with a swept bandwidth of 45 MHz (i.e., a range resolution of 3.3 m), and a Pulse Repetition Frequency (PRF) equal to 1 kHz. The passive nodes were co-located 1830 m away from the active node and used to measure the bistatic sea-clutter returns from both the horizontal and the vertical polarization. As to the geometric configuration, different bistatic angles (β) were considered by pointing the antennas at the active and passive nodes to a common clutter patch so that the intersection point between the boresight of the transmitting/receiving antennas and the position of the nodes occupy the vertices of an isosceles triangle (with axis of symmetry perpendicular to the baseline).

Table I summarizes the polarization configurations and bistatic angles (β) associated with the datasets considered in this study. Therein, the letters H and V denotes horizontal and vertical polarization, respectively.

Dataset number	Pol. Node 3 (Tx-Rx)	Pol. Node 1 (Rx)	Pol. Node 2 (Rx)	β [deg]
1	HH	H	V	60
4	HH	H	V	90
5	HH	H	V	95
8	VH	H	V	60
11	VH	H	V	90
12	VH	H	V	95

TABLE I: Polarization configurations for the considered measurements.

As to the environmental conditions (wind speed/direction and wave height/direction) they remained almost constant during the experiments (sea state 4). For all the mentioned acquisition scenarios, measurements refer to a time span of 130 s which, with a PRF of 1 kHz, corresponds to $N_s = 130000$ complex-valued slow-time samples for each range cell. In the following, before proceeding with data analysis the available slow-time measurements are suitably pre-processed so as to remove possible DC offset and imbalance between the quadrature channels [9].

III. Homogeneity Assessment

In this section, the homogeneity of the available measurements over the slow-time dimension is assessed via the Generalized Inner Product (GIP) [10]–[13]. This is a quadratic form commonly used in radar signal processing to assess whether a set of statistically independent zero-mean complex-valued Gaussian random vectors is homogeneous, i.e., to establish if they share the same spectral properties. Precisely, given K independent and identically distributed N-dimensional data vectors $\boldsymbol{x}_k \sim \mathcal{CN}(0, \boldsymbol{\Sigma}) \in \mathbb{C}^{N\times 1}$, $k = 1, \ldots, K \geq N$, the homogeneity property can be assessed relying on the following considerations

1) $\boldsymbol{\Sigma}$ can be estimated according to the Maximum Likelihood (ML) criterion via the Sample Covariance Matrix (SCM), defined as
$$\hat{\boldsymbol{\Sigma}} = \frac{1}{K}\sum_{k=1}^{K} \boldsymbol{x}_k \boldsymbol{x}_k^{\dagger}, \tag{1}$$
2) the GIP statistics, defined by the following quadratic forms
$$\xi_k = \frac{1}{K}\boldsymbol{x}_k^{\dagger}\hat{\boldsymbol{\Sigma}}^{-1}\boldsymbol{x}_k, \quad k = 1, \ldots, K, \tag{2}$$
follow a complex central Beta-distribution with shape parameters N and $M = K - N$, i.e., $\xi_k \sim \mathcal{CB}_{N,M}$, $k = 1, \ldots, K$.

Leveraging (2), the following proposition follows:

Proposition 1. *Let us consider K statistically independent data vectors. A necessary condition for the measurements $\boldsymbol{x}_k \in \mathbb{C}^{N\times 1}$, $k = 1, \ldots, K$, $K \geq N$, to be modelled as homogeneous zero-mean circularly symmetric complex Gaussian random vectors is that the quadratic forms ξ_k, $k = 1, \ldots, K$, are distributed according to a $\mathcal{CB}_{N,K-N}$ model.*

Applying this framework to the multistatic/polarimetric data collected by using the NetRAD system it is possible to study their homogeneity properties. As a preliminary remark, let us observe that in [5] it has been shown that within the coherence time both the monostatic and bistatic NetRAD measurements comply with the SIRP model, i.e., within the coherence time they can be deemed as locally Gaussian. Precisely, denoting by $z(t)$ the continuous time version of the signal collected at the ith sensor of the NetRAD system, it can be expressed as
$$z(t) = sg(t), \quad t \in T_c, \tag{3}$$
where s represents the texture component modelled as a nonnegative random variable over the coherence time, $g(t)$ denotes the speckle component described as a zero-mean circularly symmetric Gaussian process, and T_c is the coherence time. However, the analyses performed in [5] require the use of uncorrelated slow-time samples and thus no inference has been made on the possible stationarity of the speckle component (due to Gaussianity it is just necessary to study the covariance matrix stationarity as it implies the strict stationarity of the process).

In the following, the study conducted in [5] is complemented accounting for possible correlations of the slow-time samples composing the observation vector. To this end, let us denote by
$$\{\boldsymbol{z}_{i,k}\}_{k=1}^{K}, \quad i = 1, 2, 3,$$

a set of K data vectors containing N consecutive slow-time samples collected from a given range cell at the ith node. To ensure uncorrelation and statistical independence of the data vectors $\boldsymbol{z}_{i,k}$, $k = 1, \ldots, K$, $i = 1, 2, 3$, they are spaced in the slow-time domain according to the average decorrelation time of 0.05 s [5] which, at PRF of 1 kHz, corresponds to a minimum temporal lag between two observation vectors of $\Delta = 50$ samples. Precisely, denoting by $\boldsymbol{z}_i \in \mathbb{C}^{N_s \times 1}$ the available measurements in the slow-time dimension acquired at the ith sensor, the set of K data vectors can be selected as follows

$$\boldsymbol{z}_{i,k,l} = [\boldsymbol{z}_i(\Delta_{k,l} + 1), \ldots, \boldsymbol{z}_i(\Delta_{k,l} + N)]^T \in \mathbb{C}^{N \times 1}, \quad (4)$$

$k = 1, \ldots, K$, $l = 1, 2, \ldots, L$, where

- the index l allows the selection of L different sets of K data vectors from the available N_s slow-time samples, that is
$$L = \left\lfloor \frac{N_s - N + \Delta}{K\Delta} \right\rfloor ;$$
- for a given (k, l)-pair $\Delta_{k,l} = [(l-1)K + k - 1]\Delta$, allows the selection of the kth data vector for the lth data selection;
- $(K\Delta/\text{PRF}) < T_c$, i.e., for each data selection the K data vectors are picked up within the coherence time.

Figure 1 shows a pictorial representation of the data selection procedure with reference to the first set of K data vectors, i.e., considering $l = 1$.

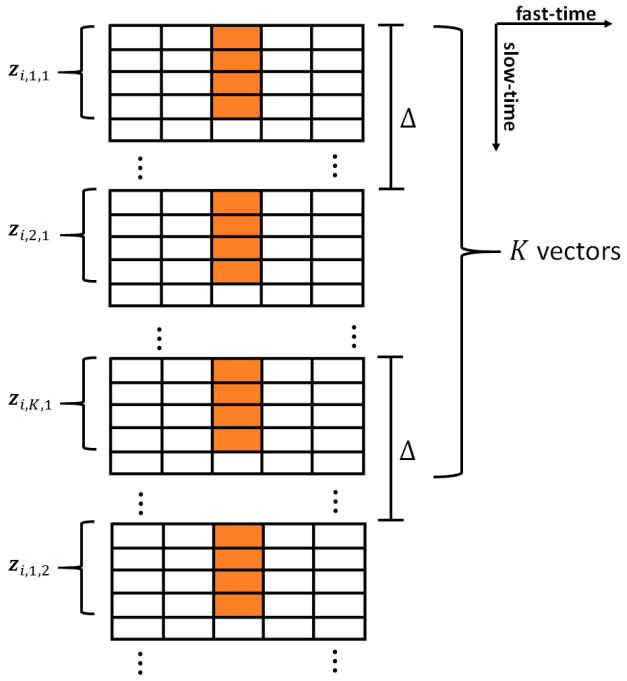

Fig. 1: Pictorial representation of the data selection procedure.

Using this data selection procedure, for a given range cell the GIP statistics can be computed according to Algorithm 1. Thus, relying on Proposition 1 the homogeneity of the data can be studied by comparing the Cumulative Distribution Function (CDF) of a $\mathcal{CB}_{N,M}$ random variable with the Empirical CDF (ECDF) of the GIP statistics. This analysis can be conducted via a visual comparison between the theoretical and the actual CDFs, and/or by testing the simple hypotheses

$$H_0^{(i,k)} : \xi_{i,k} \text{ has the CDF } F_X \,, \quad (5)$$

with $X \sim \mathcal{CB}_{N,M}$, $k = 1, \ldots, K$, and $i = 1, 2, 3$. In the following sub-sections, both the studies are performed considering the datasets 1, 4, 5, 8, 11, 12, and assuming $N = 8$ and $K = 2N$.

Algorithm 1 Procedure to compute the GIP statistics for a given range cell.

Require: $\boldsymbol{z}_{i,k,l}$, $i = 1, 2, 3$, $k = 1, \ldots, K$, $l = 1, \ldots, L$;

Ensure: GIP statistics for a given range cell;

1: set $l = 0$;

2: **repeat**

3: set $l = l + 1$;

4: compute the SCM

$$\hat{\boldsymbol{\Sigma}}_{i,l} = \frac{1}{K} \sum_{k=1}^{K} \boldsymbol{z}_{i,k,l} \boldsymbol{z}_{i,k,l}^{\dagger}, \quad i = 1, 2, 3 \,;$$

5: compute the quadratic forms

$$\xi_{i,k,l} = \frac{1}{K} \boldsymbol{z}_{i,k,l}^{\dagger} \hat{\boldsymbol{\Sigma}}_{i,l}^{-1} \boldsymbol{z}_{i,k,l}, \quad i = 1, 2, 3, \quad k = 1, \ldots, K;$$

6: **until** $l \leq L$

A. Analysis via Visual Inspection

The aim of this analysis is to visually compare the theoretical and the empirical CDF of the GIP statistics. To this end, for a given sensor/range cell pair, the ECDF is computed starting from the samples

$$\boldsymbol{\xi}_i^{CV} = [\boldsymbol{\xi}_{i,1}^{CV}, \ldots, \boldsymbol{\xi}_{i,L}^{CV}], \quad i = 1, 2, 3 \,, \quad (6)$$

where

$$\boldsymbol{\xi}_{i,l}^{CV} = [\xi_{i,1,l}, \ldots, \xi_{i,K,l}], \quad l = 1, \ldots, L, \quad i = 1, 2, 3 \,. \quad (7)$$

For each dataset, Figure 2 displays the ECDF together with the theoretical CDF. Precisely, considering the ith sensor, each plot displays an ECDF for a given range cell. By visual inspection of the curves it is possible to observe that

- regardless of the considered dataset/range cell the ECDF associated with the bistatic measurements achieves a good agreement with the theoretical model;
- the ECDF corresponding to the horizontally co-polarized bistatic measurements are closer than the monostatic counterparts to the theretical model (see Figure 2(a), (c), and (d)).

The last behaviour can be further assessed by the means of the Cramer Von Mises (CV) distance. This is an integral

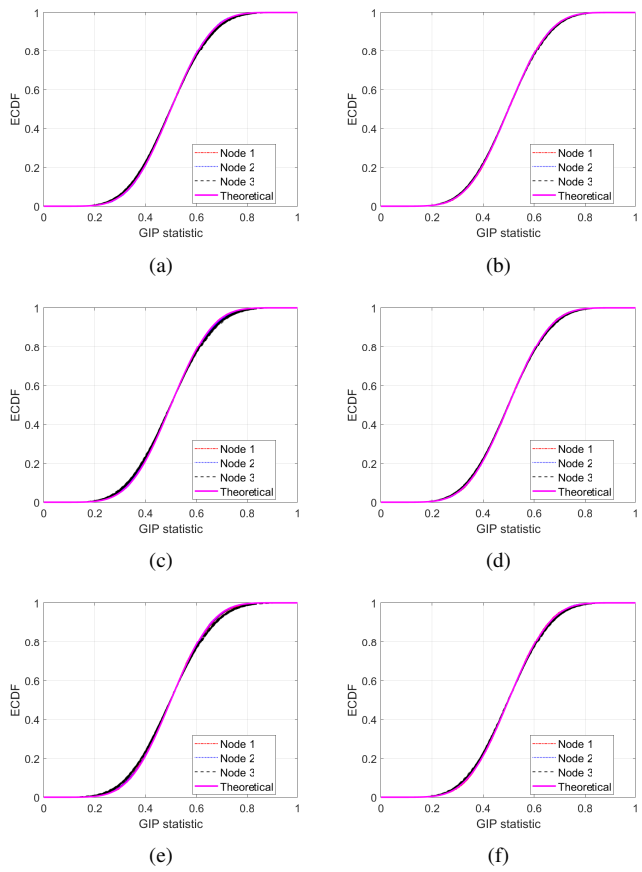

Fig. 2: ECDFs evaluated using the GIP statistic for the three nodes: (a) dataset 1, (b) dataset 8, (c) dataset 4, (d) dataset 11, (e) dataset 5, (f) dataset 12.

distributional distance between two CDFs and given a set of H identically distributed observations $[X_1, \ldots, X_H]$ of the random variable X, it can be calculated as

$$d_{CV} = \frac{1}{12H} + \sum_{h=1}^{H} \left| F_X(X_{(h)}) - \frac{2h-1}{2H} \right|^2 , \qquad (8)$$

where $F_X(\cdot)$ is the CDF of the design distribution and $X_{(h)}$ is the hth order statistic from the set of random variables. Using this metric, Table II reports the mean CV distance obtained by averaging the values of d_{CV} computed for each range cell of the clutter patch. The values confirms that for the horizontally co-polarized case (datasets 1, 4, and 5), the mean CV distance for the monostatic measurements is higher than the bistatic counterpart. Interestingly, for this configuration it is also possible to observe that the CV distance increases as the distance between the monostatic node and the clutter patch reduces. Indeed, since for the NetRAD system the position of the nodes is fixed, the distance between the sensors and the clutter patch reduces as the bistatic angle increases.

B. Analysis via Hypothesis Testing

The aim of this analysis is to verify whether the GIP statistics follow a $\mathcal{CB}_{N,M}$ model by testing the simple hypotheses in (5). The study is conducted by the means of the Kolmogorov-Smirnov (KS) test which is based on the maximum difference between the supposed and the empirical CDFs of the data, called the KS statistic. In particular, for a given range cell the KS statistic in (5) is computed using the samples

$$\boldsymbol{\xi}_{i,k}^{KS} = [\xi_{i,k,1}, \ldots, \xi_{i,k,L}], \quad i = 1,2,3, \quad k = 1, \ldots, K\,. \qquad (9)$$

Applying the KS test to the considered problem, Table III shows the average percentage of GIP statistics for which the $\mathcal{CB}_{N,M}$ distribution cannot be rejected for a 0.01 significance level. Precisely, for each sensor and a given range cell the samples $\boldsymbol{\xi}_{i,k}^{KS}$, $i = 1,2,3$, $k = 1, \ldots, K$, are used to perform K different KS test. Then, the results are averaged with respect to both the number of data vectors and range cells. Results pinpoints that within the coherence time the considered measurements can be deemed as homogeneous (i.e., stationary) and locally Gaussian (as predicted by the SIRP model). In other words, within the coherence time for both the monostatic and bistatic sensors the received data can be modelled as a zero-mean circularly symmetric complex Gaussian random vectors with a specific covariance matrix, which can be possibly different from one sensor to another.

Dataset	Node 1	Node 2	Node 3
1	0.14	0.09	1.28
8	0.08	0.09	0.29
4	0.19	0.24	2.81
11	0.11	0.11	0.67
5	0.24	0.11	3.97
12	0.11	0.24	0.87

TABLE II: Average CV distance.

Dataset	Node 1	Node 2	Node 3
1	99.1	98.9	98.3
8	99.0	99.0	98.8
4	98.8	98.9	97.5
11	98.9	99.0	98.5
5	98.9	99.0	97.8
12	99.0	98.9	98.7

TABLE III: Percentage of GIP statistics for which the Beta distribution cannot be rejected for a 0.01 significance level.

IV. Covariance Matrix Structure Classification

The analysis of Section III revealed that within the coherence time the available multistatic/polarimetric measurements can be deemed as homogeneous zero-mean circularly symmetric complex Gaussian random vectors, i.e., they are locally Gaussian and stationary. However, no inferences can be made over a time scale greater than the coherence time or about the spectral characteristics of the sea-clutter perceived at different sensors or polarizations. In this respect, some understanding can be gained by studying the structure of the covariance matrix of the speckle component over successive coherence time intervals. Indeed, for a given sensor a necessary condition for the data observed over different coherence time intervals to share the same spectral characteristics (up to a scale factor

representing the texture component) is that the covariance matrix of the corresponding speckle components shares the same structure. Moreover, specific structures such as hermitian unstructured, symmetric unstructured, centrohermitian, and centrosymmetric, can provide interesting insights about the spectral behaviour of the clutter perceived at different sensors. As a matter of fact, centrosymmetry or centrohermitianity are necessary conditions for the observations to be deemed as Wide Sense Stationary (WSS). Besides, for a symmetric or a centrosymmetric structure the Power Spectral Density (PSD) of the clutter has to exhibit symmetric behaviour with respect to the zero-Doppler frequency. For instance, by describing the sea-clutter PSD with the well established Gaussian-shaped model, the generic (r, c) entry of the covariance matrix of the speckle component over a coherence time interval can be expressed as

$$\boldsymbol{M}(r,c) = \alpha \rho^{(r-c)^2} e^{j2\pi(r-c)f_d}, \quad (r,c) \in \{1,\dots,N\}^2, \tag{10}$$

where N is the number of pulses in the Coherent Processing Interval (CPI), α is a real-valued positive parameter, ρ is the one-lag correlation coefficient, and f_d represents the normalised Doppler frequency of the sea-clutter. Thus, a real-valued covariance matrix (symmetric unstructured/centrosymmetric) can be associated to observation with a zero-Doppler frequency. Conversely, complex-valued covariance matrices (hermitian/centrohermitian) are representative of clutter returns with a non zero-Doppler frequency.

Based on the previous considerations, the aim of this section is to infer about the structure of the covariance matrix of the speckle component for both the monostatic and the bistatic sea-clutter measurements. To this end, relying on the framework prposed in [14], for a given sensor and exploiting observations from a specific coherence time interval, covariance symmetries can be studied considering the following hypotheses test

$$\begin{cases} H_1 : \boldsymbol{M} \in \mathbb{C}^{N\times N} & \text{is Hermitian unstructured,} \\ H_2 : \boldsymbol{M} \in \mathbb{R}^{N\times N} & \text{is symmetric unstructured,} \\ H_3 : \boldsymbol{M} \in \mathbb{C}^{N\times N} & \text{is centrohermitian,} \\ H_4 : \boldsymbol{M} \in \mathbb{R}^{N\times N} & \text{is centrosymmetric,} \end{cases} \tag{11}$$

where the number of unknown parameters under each hypothesis is given by

$$\begin{cases} m_1 = N^2 & \text{under } H_1, \\ m_2 = N(N+1)/2 & \text{under } H_2, \\ m_3 = N(N+1)/2 & \text{under } H_3, \\ m_4 = \begin{cases} \dfrac{N}{2}\left(\dfrac{N}{2}+1\right) & \text{if } N \text{ is even} \\ \left(\dfrac{N+1}{2}\right)^2 & \text{if } N \text{ is odd} \end{cases} & \text{under } H_4. \end{cases} \tag{12}$$

To screen among the different hypotheses suitable strategies can be considered which involve the use of the log-likelihood function of the observations and an estimate of the covariance matrix under each hypothesis [14]. As to the former, since the analyses are performed within the coherence time the observations can be modelled according to a zero-mean complex Gaussian model. As to the latter, instead, assuming the availability of $K \geq N$ independent data vectors $\boldsymbol{Z} = [\boldsymbol{z}_1, \dots, \boldsymbol{z}_K] \in \mathbb{C}^{N\times K}$, under the ith hypothesis the ML estimate of the covariance matrix of the speckle component is given by

$$\begin{cases} \hat{\boldsymbol{M}}_1 = \dfrac{1}{K}\boldsymbol{Z}\boldsymbol{Z}^\dagger & (\text{Under } H_1), \\ \hat{\boldsymbol{M}}_2 = \dfrac{1}{K}\Re\left\{\boldsymbol{Z}\boldsymbol{Z}^\dagger\right\} & (\text{Under } H_2), \\ \hat{\boldsymbol{M}}_3 = \dfrac{1}{2K}\left[\boldsymbol{Z}\boldsymbol{Z}^\dagger + \boldsymbol{J}(\boldsymbol{Z}\boldsymbol{Z}^\dagger)^*\boldsymbol{J}\right] & (\text{Under } H_3), \\ \hat{\boldsymbol{M}}_4 = \dfrac{1}{2K}\Re\left\{\boldsymbol{Z}\boldsymbol{Z}^\dagger + \boldsymbol{J}(\boldsymbol{Z}\boldsymbol{Z}^\dagger)^*\boldsymbol{J}\right\} & (\text{Under } H_4), \end{cases} \tag{13}$$

where $\boldsymbol{J} \in \mathbb{R}^{N\times N}$ is a permutation matrix such that $\boldsymbol{J}(r,c) = 1$ if and only if $r + c = N + 1$, $(r,c) \in \{1,\dots,N\}^2$. Finally, as to the classification rule the Bayesian Information Criterion (BIC) is used. This is tantamount to considering the decision rule

$$H_{\widehat{i}} = \arg\min_{i\in\mathcal{H}} \left\{-2s(\hat{\boldsymbol{M}}_i, H_i) + m_i \log(K)\right\}. \tag{14}$$

where $\mathcal{H} = \{1,2,3,4\}$, whereas $s(\hat{\boldsymbol{M}}_i, H_i)$ and $\hat{\boldsymbol{M}}_i$ are the log-likelihood function and the ML estimate of $\boldsymbol{M}_i$ under the i-th hypothesis, respectively.

The analysis is conducted using the data selection procedure specified in (4) for the measurements from datasets 1, 4, 5, 8, 11, 12, assuming $N = 8$ and $K = 2N$. Specifically, for a given sensor, L different classification instances are made along the slow-time dimension for each range cell of the clutter patch.

Table IV reports the average percentage of data classified under each hypothesis. Inspection of the results highlights that

- for both the monostatic and the bistatic data the top rated structures are centrosymmetric and centrohermitian;
- the monostatic (bistatic) returns generally exhibit a centrohermitian (centrosymmetric) covariance matrix;
- for both the monostatic and the bistatic measurements the percentage of data classified under the hypothesis 3 and 4 depends upon polarimetric/geometric configuration.

As to the last behaviour and with reference to the bistatic measurements, the obtained values also highlight that when the transmitter is horizontally polarized (datasets 1, 4, and 5), as the bistatic angle increases the percentage of data classified as centrohermitian increases while that identified as centrosymmetric reduces. For the vertically-polarized counterpart, this behaviour is limited to datasets 8 and 11 (i.e., up to bistatic angles less than or equal to 90°). Additionally, for a specific geometric configuration (i.e., datasets 1-8, 4-11, and 5-12), the percentage of data classified under the centrohermitian (centrosymmetric) hypothesis for co-polarized monostatic measurements is higher (smaller) than the value obtained for the cross-polarized counterparts.

Finally, additional analyses not reported herein for brevity show that centrosymmetry and centrohermitianity can be linked to the sea-wave profile (which depends on the sea-state).

Dataset	Node	Hyp. 1	Hyp. 2	Hyp. 3	Hyp. 4
1	1	0.01	0.12	6.58	93.29
	2	0.00	0.12	3.91	95.98
	3	0.13	0.02	75.82	24.03
8	1	0.00	0.12	3.07	96.81
	2	0.04	0.13	16.85	82.98
	3	0.11	0.06	57.06	42.78
4	1	0.02	0.09	15.91	83.98
	2	0.10	0.14	17.95	81.82
	3	0.84	0.01	95.57	3.58
11	1	0.02	0.14	10.86	88.97
	2	0.07	0.08	35.53	64.32
	3	0.27	0.01	91.25	8.47
5	1	0.04	0.14	21.56	78.25
	2	0.08	0.08	25.45	74.40
	3	0.81	0.07	96.60	2.52
12	1	0.03	0.10	10.14	89.74
	2	0.06	0.04	33.41	66.49
	3	0.14	0.00	94.21	5.65

TABLE IV: Percentage of data classified under each hypothesis.

V. Conclusions

This paper has dealt with the statistical analysis of multistatic/polarimetric sea-clutter data considering different polarimetric/geometric scenarios. Precisely, starting from the analysis conducted in [5], the study has been firstly focused on establishing whether the data can be modeled as drawn from a stationary process, i.e., if they are homogeneous within the coherence time. To this end, relying on suitable GIP-based statistics some necessary conditions for the data to be homogeneous have been tested by the means of the KS test and CV distance. Then, the possible presence of structures in the clutter covariance matrix for both the monostatic and bistatic measurements has been investigated through ad-hoc statistical tools. Analysis has shown that, regardless the polarimetric and geometry configuration within the coherence time the data can be modeled as drawn from a stationary process. The analysis has also revealed that the structure of the covariance matrix associated with the speckle depends upon the polarimetric/geometric configuration of the system. Additionally, the monostatic (bistatic) returns generally exhibit a centrohermitian (centrosymmetric) covariance matrix.

The obtained results provide a further experimental evidence on the mutistatic/polarimetric clutter diversity as a function of both environment conditions and polarimetric/geometric configuration of the system. A possible future research direction involves the possible presence of relationships between the statistical parameters characterizing the returns on the different channels (such as the proportionality between the clutter covariance matrices on the two bistatic polarimetric channels). This study is undoubtedly of interest towards the design of bespoke detection strategies relying on the joint use of both monostatic and bistatic measurements.

Acknowledgements

The work of V. Carotenuto was supported by the research program PON R&I AIM1878982-1. The work of A. Aubry and A. De Maio was partially supported by the European Union under the Italian National Recovery and Resilience Plan (NRRP) of NextGenerationEU, partnership on "Telecommunications of the Future" (CUP J33C22002880001, PE00000001 - program RESTART). The authors are grateful to the UCL and UCT team for collecting the data and making them available for this analysis.

References

[1] M. A. Richards, J. A. Scheer, and W. A. Holm, Eds., *Principles of Modern Radar: Basic principles*, ser. Radar, Sonar & Navigation. Institution of Engineering and Technology, 2010.

[2] A. Aubry, A. De Maio, and A. Farina, Eds., *Polarimetric Radar Signal Processing*, ser. Radar, Sonar and Navigation. Stevenage, England: Institution of Engineering and Technology, February 2023.

[3] H. D. Griffiths, "Keynote address: clutter diversity: A new degree of freedom in multistatic radar," in *2014 IEEE Radar Conference*, 2014, pp. 11–11.

[4] R. Klemm, U. Nickel, C. Gierull, P. Lombardo, H. Griffiths, and W. Koch, Eds., *Novel Radar Techniques and Applications Volume 2: Waveform Diversity and Cognitive Radar, and Target Tracking and Data Fusion*, ser. Radar, Sonar & Navigation. Institution of Engineering and Technology, 2017.

[5] A. Aubry, V. Carotenuto, A. De Maio, and F. Fioranelli, "Compatibility assessment of multistatic/polarimetric clutter data with the sirp model," *IEEE Transactions on Aerospace and Electronic Systems*, pp. 1–16, 2022.

[6] W. Al-Ashwal, "Measurement and modelling of bistatic sea clutter," Ph.D. dissertation, University College London, London, U.K., 2011.

[7] E. Conte and M. Longo, "Characterisation of radar clutter as a spherically invariant random process," *IEE Proceedings F (Communications, Radar and Signal Processing)*, vol. 134, pp. 191–197, April 1987.

[8] F. Fioranelli, M. Ritchie, H. Griffiths, S. Sandenbergh, and M. Inggs, "Analysis of polarimetric bistatic sea clutter using the netrad radar system," *IET Radar, Sonar & Navigation*, vol. 10, no. 8, pp. 1356–1366, 2016.

[9] J. T. Nohara, "Detection of growlers in sea clutter using an x-band pulse-doppler radar," Ph.D. dissertation, McMaster University, 1991.

[10] M. Rangaswamy, J. H. Michels, and B. Himed, "Statistical analysis of the non-homogeneity detector for stap applications," *Digital Signal Processing*, vol. 14, no. 3, pp. 253–267, 2004.

[11] M. C. Wicks, Y. Zhang, and R. Schneible, "A generalized inner product based algorithm for improved detection and discrimination of over resolved targets in mimo radar," in *8th European Conference on Synthetic Aperture Radar*, 2010, pp. 1–4.

[12] W. Melvin, M. Wicks, and R. Brown, "Assessment of multichannel airborne radar measurements for analysis and design of space-time processing architectures and algorithms," in *Proceedings of the 1996 IEEE National Radar Conference*, 1996, pp. 130–135.

[13] C. Teixeira, J. Bergin, and P. Techau, "Adaptive thresholding of non-homogeneity detection for stap applications," in *Proceedings of the 2004 IEEE Radar Conference (IEEE Cat. No.04CH37509)*, 2004, pp. 355–360.

[14] V. Carotenuto, A. De Maio, D. Orlando, and P. Stoica, "Model order selection rules for covariance structure classification in radar," *IEEE Transactions on Signal Processing*, vol. 65, no. 20, pp. 5305–5317, 2017.